Chemical Geology 422 (2016) 13–24

Contents lists available at ScienceDirect

Chemical Geology

journal homepage: www.elsevier.com/locate/chemgeo

Extracting thermal histories from the near-rim zoning in titanite using coupled U-Pb and trace-element depth profiles by single-shot laser-ablation split stream (SS-LASS) ICP-MS

M.A. Stearns *, J.M. Cottle, B.R. Hacker, A.R.C. Kylander-Clark

Department of Earth Science, UC Santa Barbara, 1006 Webb Hall Santa Barbara, CA 93106-9630

ARTICLE INFO

Article history:
Received 25 September 2015
Received in revised form 18 December 2015
Accepted 22 December 2015
Available online 29 December 2015

Keywords:
Diffusion
Titanite
LA-ICP-MS
U-Pb
Petrochronology
Zr thermometry
Pamir Plateau

ABSTRACT

A method for depth profiling using single-shot laser-ablation split stream (SS-LASS) ICP-MS is developed to simultaneously measure U-Pb age and trace-element concentrations in titanite. Simple semi-infinite, 1-D half-space diffusion models were applied to near-rim, trace-element zoned domains in titanite to distinguish between cooling and (re)crystallization ages and investigate the potential for preservation of thermally mediated diffusive loss profiles. These data illustrate the need to measure multiple trace elements with varying diffusivities to interpret a mineral's thermal history resulting from the non-unique nature of 1-D diffusion models where both temperature and time are unknown. A case study of titanites from two Pamir Plateau gneiss domes indicates they underwent ≥25 Myr of amphibolite and granulite facies metamorphism yet did not experience significant volume diffusion modification following (re)crystallization. The interpretation of prolonged (re)crystallization rather than diffusion allows for high-resolution, near-rim temperature-time histories to be extracted using U-Pb dates and Zr^{4+} apparent temperatures by SS-LASS.

1. Introduction

Core-to-rim elemental and isotopic zoning in minerals has been widely used to quantify rates of geologic processes (e.g. Dodson, 1973; Chakraborty, 2006). Much of this work has centered on electron-microprobe analysis (EPMA) of variations in elemental abundances, which are typically interpreted using laboratory-determined volume diffusivities (e.g., Cherniak, 1993, 2006). Isotopic zoning in minerals has generally been harder to measure because of limitations in spatial resolution, but major advances have been made with secondary-ion mass spectrometry (SIMS), particularly in the measurement and interpretation of isotopic and chemical-zoning measured as a depth profile by sputtering from the grain rim inward (Lee et al., 1997; Grove and Harrison, 1999; Abbott et al., 2012; Kelley et al., 2014). The application of inductively coupled plasma mass spectrometry (ICP-MS) to depth profiling heralds a new era because of its ability to more rapidly and easily measure multiple isotopes and elements near-simultaneously (e.g., Kohn and Corrie, 2011; Smye and Stockli, 2014). Additionally, the development of laser-ablation split stream (LASS) ICP-MS, which enables simultaneous measurement of U/Th-Pb isotopic ratios and trace-element concentrations, has yet to be applied to depth profiling of minerals. One of the biggest advantages to the simultaneous measurement of multiple elements is the ability to use elements with radically different diffusive length-scales as a tool for assessing whether zoning resulted from thermally mediated volume diffusion or other processes such as recrystallization.

This paper showcases a new technique, combining the high spatial resolution of single shot (SS)-LA-ICP-MS (Cottle et al., 2009, 2012; Viete et al., 2015) with the high-resolution, multi-isotope/element measurement capabilities of laser-ablation split stream (LASS; Kylander-Clark et al., 2013) to resolve U-Pb age and trace-element zoning in titanite at the ~100 nm scale (Fig. 1). Several secondary reference titanites were analyzed in addition to natural samples to demonstrate the external reproducibility of the SS-LASS technique. Data are then used to interpret the elemental and isotopic variation and extract the thermal histories of two titanites from the Pamir Plateau. Titanite is an especially useful tool for dating petrologic processes (e.g., Rubatto and Hermann, 2001; Parrish et al., 2006; Spencer et al., 2013) because it is present in a variety of bulk compositions (Frost et al., 2001), recrystallizes and grows via net-transfer reactions at amphibolite and granulite-facies metamorphic conditions (Spear, 1981; Harlov et al., 2006), contains compositional variation that can be linked to changes in major-phase abundance (Prowatke and Klemme, 2005), has a calibrated Zr^{4+} thermometer (Hayden et al., 2008) and has experimentally determined Pb and Zr diffusion rates (Cherniak, 1993, 2006). Available experimental data predict that Pb and Zr have quite different diffusivities and should diffuse significantly different distances (Pb should diffuse ~14x farther than Zr over the same period of time) at temperatures of ~600–700 °C over millions of years (Cherniak,

* Corresponding author.
E-mail address: michael.stearns@utah.edu (M.A. Stearns).

http://dx.doi.org/10.1016/j.chemgeo.2015.12.011
0009-2541/

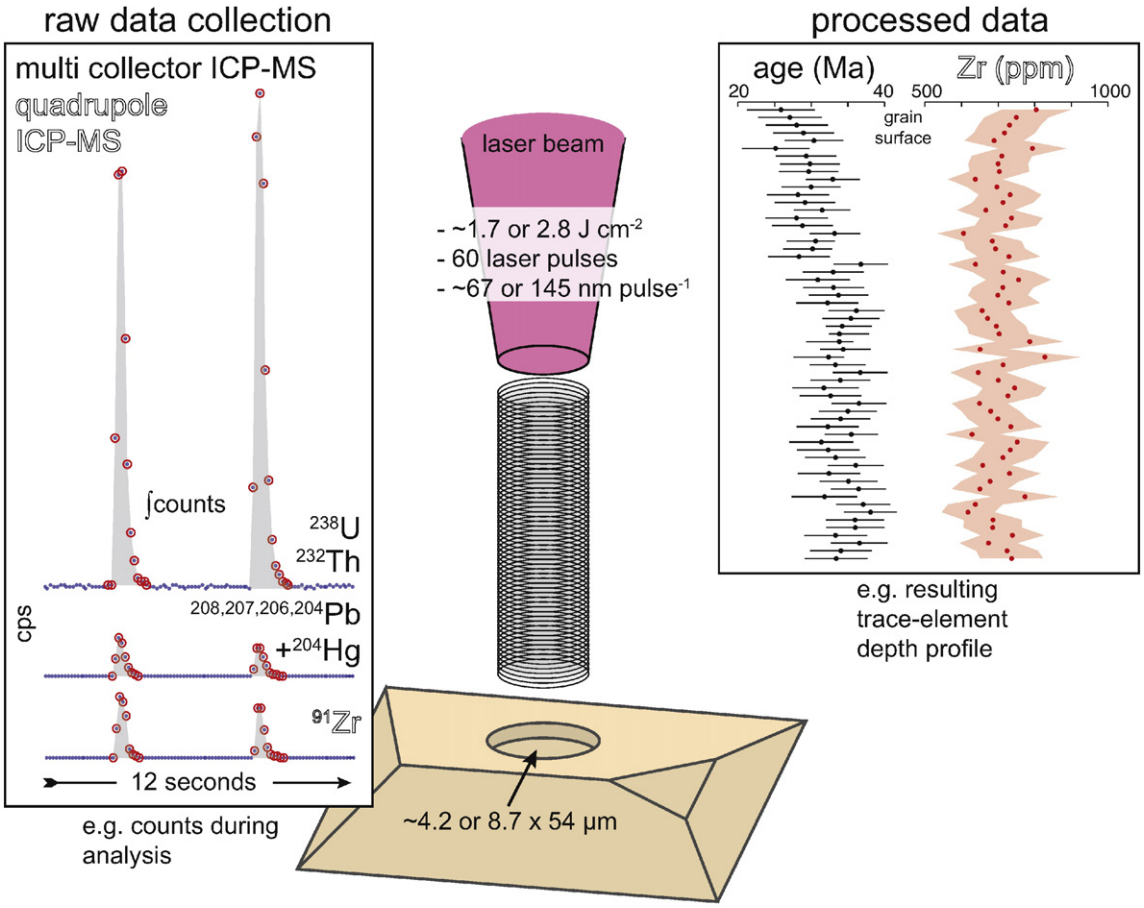

Fig. 1. Depth profiling of titanite via single-shot laser-ablation split stream (SS-LASS) consists of a number of single laser pulses that are simultaneously fed into a quadrupole-ICP-MS to measure Zr concentration and a multicollector-ICP-MS to measure the total counts of U, Th, and Pb. Isotopic compositions and concentrations are then calculated normalized to the primary standards. Each 54 μm diameter SS-LASS datum consists of ~150–330 μm3, 5,500–11,800 ng of titanite, and ~0.3–0.6 ng of Pb (50 ppm; or ~0.05–0.1 ng for 10 ppm Pb) compared to traditional analysis of a 40 μm diameter spot fired 80 times, which corresponds to ~6,700 μm3, ~240,000 ng of titanite, ~12 ng of Pb (50 ppm; ~2.4 ng for 10 ppm Pb).

2006). There is some question about the applicability of experimental diffusion data to natural rocks, however, with a number of studies examining natural titanite and concluding that Pb and Zr are immobile under such temperatures (Scott and St-Onge, 1995; Zhang and Schärer, 1996; Kohn and Corrie, 2011; Spencer et al., 2013; Stearns et al., 2015). The aim of this study is not to quantify the discrepancy between

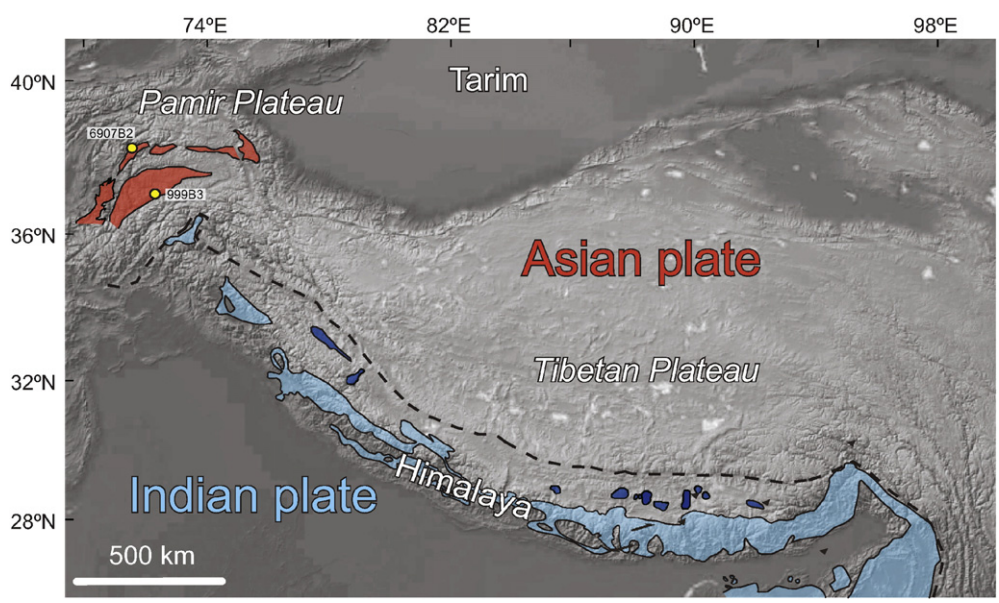

Fig. 2. The Pamir Plateau is the most extensive exposure of the Cenozoic, Asian mid–deep crust in the India–Asia collision zone. The locations of samples 6907B2 and 999B3 (yellow dots) are within Yazgulem and Shakhdara domes, respectively. The Yazgulem dome is dominated by metamorphosed siliciclastic and carbonate rocks that were intruded by plutons during shortening. Alternatively, the Shakhdara dome is predominantly granitoids and orthogneisses that have been penetratively deformed during large-magnitude extension related to exhumation. Figure modified from Stearns et al. (2013).

experimental- and empirically-derived diffusion data, but rather to highlight a method for characterizing near-rim isotopic and chemical zoning and comparing it to models of lattice diffusion. The method outlined here allows for extracting robust thermochronometry records from titanites with near-rim elemental and isotopic zoning. (See Fig. 2.)

It is not uncommon for titanite grains to preserve intragrain variation of U-Pb dates and Zr concentrations (Kohn and Corrie, 2011; Bonamici et al., 2015; Stearns et al., 2015). Understanding whether this variation resulted from lattice diffusion, neocrystallization, or recrystallization is important for interpreting the titanite petrochronology. The spatial patterns of in situ dates and trace element analyses — in conjunction with the grain size distribution of the chronometer phase — can assess the probability of lattice diffusion-controlled closure as a resetting mechanism (Stearns et al., 2015). For example, samples with a range of grain sizes that define a single population of U-Pb dates must record a single neocrystallization age or complete recrystallization because of the quadratic dependence of lattice diffusion on distance/grain size. Put simply, small grains should be younger/have lower concentrations than big grains and spot analyses should young/have lower concentrations towards the rims of grains. Alternatively, samples that have a uniform grain size distribution and/or a spatially coherent range of U-Pb dates are equivocal could result from either diffusive equilibration or uniform (re)crystallization processes. The latter situation requires further microanalysis and modeling to understand whether the near surface isotopic and chemical variation record (re)crystallization or lattice diffusion controlled closure.

2. Methods

2.1. Sample Selection and Geologic Setting of the Pamir Titanites

Natural samples analyzed in this study come from the Pamir Plateau, a region that exposes middle to deep crustal rocks related to the India-Asia collision. The rocks from the middle to deep crust crop out in two groups of genetically related gneiss domes (Schwab et al., 2004). The now-exhumed middle to deep crust experienced amphibolite and granulite facies metamorphism (Schmidt et al., 2011) lasting at least ≥15 Myr from ~35–8 Ma (Stübner et al., 2013; Smit et al., 2014; Stearns et al., 2013, 2015). Titanites from these domes record U-Pb ages spanning ~30 Myr and 2) elevated Zr-in-titanite temperatures. This record spans both prograde and retrograde metamorphism within the domes (Stearns et al., 2015). Samples 6907B2 and 999B3 were chosen to investigate the near-rim isotopic and chemical variation at a length scale less than the spot diameter of a traditional LA-ICP analysis (~30–40 μm).

Sample 6907B2 is a undeformed granodiorite emplaced near the northern margin of Yazgulem dome. The granitoids intruded during thickening of the Pamir crust related to the collision of India and predate peak metamorphism and exhumation of the mid–deep crust within the Yazgulem dome. Titanite from 6907B2 are typically euhedral and range from ~300–400 μm in diameter. Titanites dated by traditional U-Pb LA-ICP-MS form a single population age of 40.1 ± 0.8 Ma (MSWD = 1.1; Stearns et al., 2015). The Yazgulem dome experienced prograde metamorphism from ~27–20 Ma (Smit et al., 2014) followed by rapid exhumation from ~20–16 Ma recorded by monazite, titanite (Stearns et al., 2013, 2015), and multiple thermochronometer systems (Rutte et al., 2014).

Sample 999B3 is a garnet amphibolite boudin from the southern margin of the Shakhdara dome. The sample contains relict pyroxene and is interpreted to have been overprinted by retrograde metamorphism during exhumation of the Shakhdara dome beginning at ~20 Ma (Stearns et al., 2015). Most titanites from 999B3 are subhedral to anhedral and range in size from ~150–400 μm in diameter. A subhedral grain with pristine crystal faces was chosen for this study to ensure characterization of the actual grain rim. Sample 999B3 has not been dated by traditional LA-ICP-MS analysis, but U-Pb titanite ages from lithologically and structurally similar rocks nearby range in age from ~17–9 Ma (Stearns et al., 2015). The Shakhdara dome experienced prograde metamorphism from ~37 Ma followed by a prolonged exhumation recorded by titanite from ~20–8 Ma (Stübner et al., 2013; Stearns et al., 2015).

Both 999B3 and 6907B2, contain titanite grains with near-rim U-Pb isotopic and trace element variation that resemble (i.e. a Gaussian decrease from grain mantle to grain rim) thermally-mediated diffusional loss of Pb and Zr. Whether this type of near-surface variation records mineral closure or (re)crystallization is important for interpreting the titanite record of metamorphism in both the Pamir and for application of titanite to petrochronology studies in general.

2.2. Sample preparation

Well-characterized titanites from Fish Canyon tuff (FC-1; 28.53 ± 0.05 Ma; Schmitz and Bowring, 2001), Y1710C5 (391.8 ± 2.7 Ma; Spencer et al., 2013), Bear Lake Ridge (BLR-1; 1047.1 ± 0.4 Ma; Aleinikoff et al., 2007; Mazdab, 2009), Ontario-2 (ONT-2; 1053.3 ± 3.1 Ma; Spencer et al., 2013), and NIST-610 glass (Gao et al., 2002) were mounted in epoxy and polished to medial sections. Whole, subhedral to euhedral titanite crystals from two Pamir rocks, 6907B2 and 999B3, known to have variation in either age or trace-element content were mounted in the same 25-mm diameter epoxy mount such that pristine external crystal faces were exposed at the mount surface without polishing. The grains were inspected both by optical reflected light and scanning electron microscope to ensure the integrity of the crystal faces following mineral separation. No polishing was performed prior

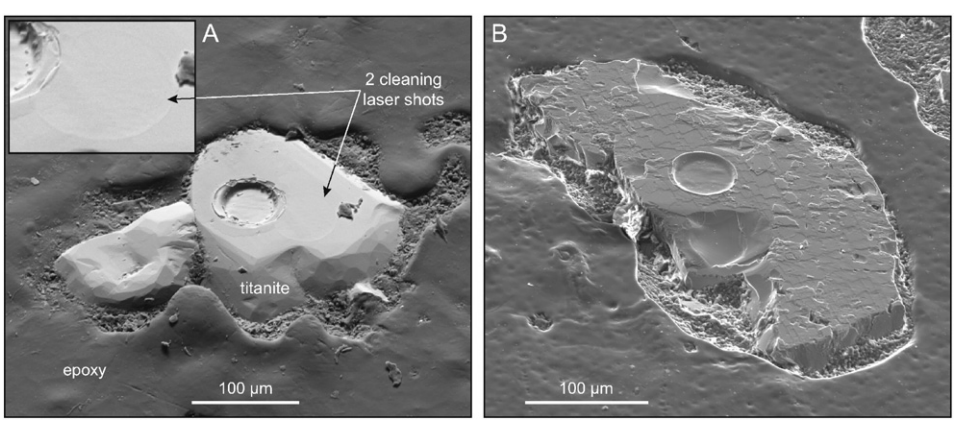

Fig. 3. Oblique secondary electron images of pristine, unpolished titanite grains from sample A) sample 6907B2 and B) sample 999B3 shows the 1) ideal flat pit bottom from homogenous laser ablation and the high aspect ratio of the final laser pit, which produces consistent single-shot sampling and mitigates the effects of downhole fractionation. The laser was fired twice prior to analysis (shown by arrow and inset detail) to clear the surfaces of the grains of contamination.

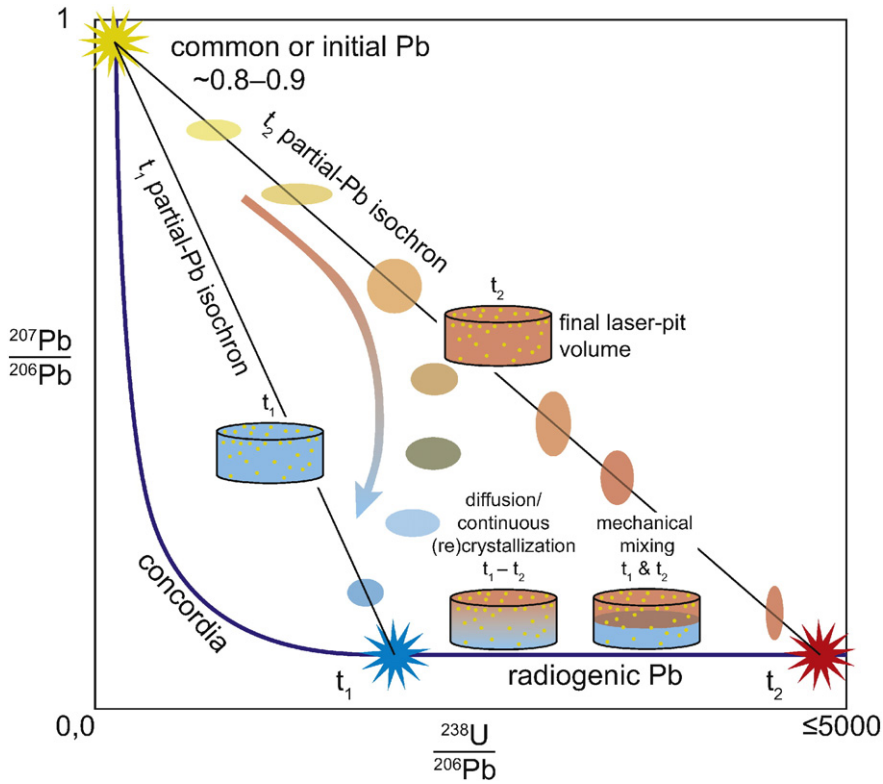

Fig. 4. The incorporation of non-radiogenic Pb (high $^{207}Pb/^{206}Pb$, low $^{238}U/^{206}Pb$) into titanite during crystallization, and the resulting mixing with radiogenic Pb (low $^{207}Pb/^{206}Pb$, high $^{238}U/^{206}Pb$), necessitates the use of a Tera-Wasserburg concordia plot and the calculation of partial-Pb isochrons or intercept ages (Ludwig, 1998). Analyses can be evaluated for different proportions of two or more end-member Pb compositions, a non-radiogenic Pb and one or more radiogenic Pb compositions, based on the trajectory of the data and position within the depth profile.

to analysis, but mounts were thoroughly cleaned with distilled water prior to analysis.

2.3. Analysis

A 193 nm Photon Machines ArF excimer laser equipped with a two-volume Helex® laser cell was used with 0.25 l min^{-1} He total and 1.15 l min^{-1} Ar carrier-gas flow per mass spectrometer. The relative gas flows to each instrument were tuned to maximize sensitivity prior to analysis. The typical washout time following a laser pulse was less than 1 s and 8–10 s of background was collected between laser pulses. The laser parameters used were fluences of ~1.7 and 2.8 J/cm^2 corresponding to an excavation rate of ~67 and ~145 nm, respectively, and a spot diameter of 54 μm. The ablated analyte was split using a Teflon T-connector and sent to two mass spectrometers to maximize count rates: U-Pb isotopic ratios and U, Th, Pb concentrations were measured on a Nu Instruments HR Nu Plasma ICP-MS and the trace element zirconium (^{90}Zr) was measured on an Agilent 7700S quadrupole ICP-MS. A complete list of

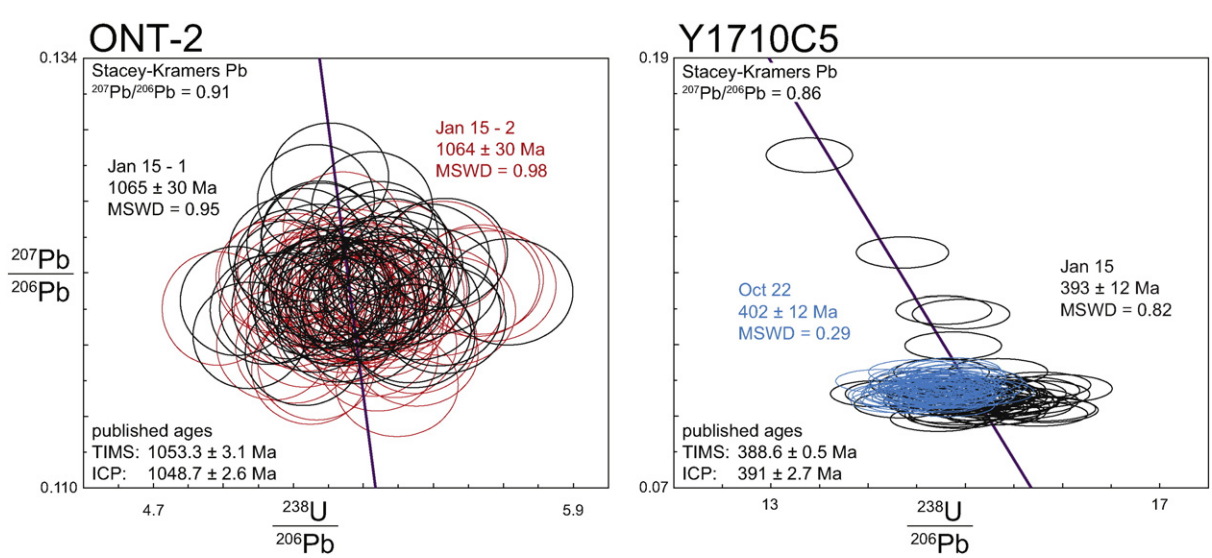

Fig. 5. Single-shot U-Pb data for the secondary reference titanites ONT-2 and Y1710C5 (Spencer et al., 2013) analyzed in run during different sessions indicate a ~3% external reproducibility of the U-Pb dating portion of the SS-LASS method, compared to ~2% external reproducibility of traditional LASS-ICP-MS analyses (Kylander-Clark et al., 2013).

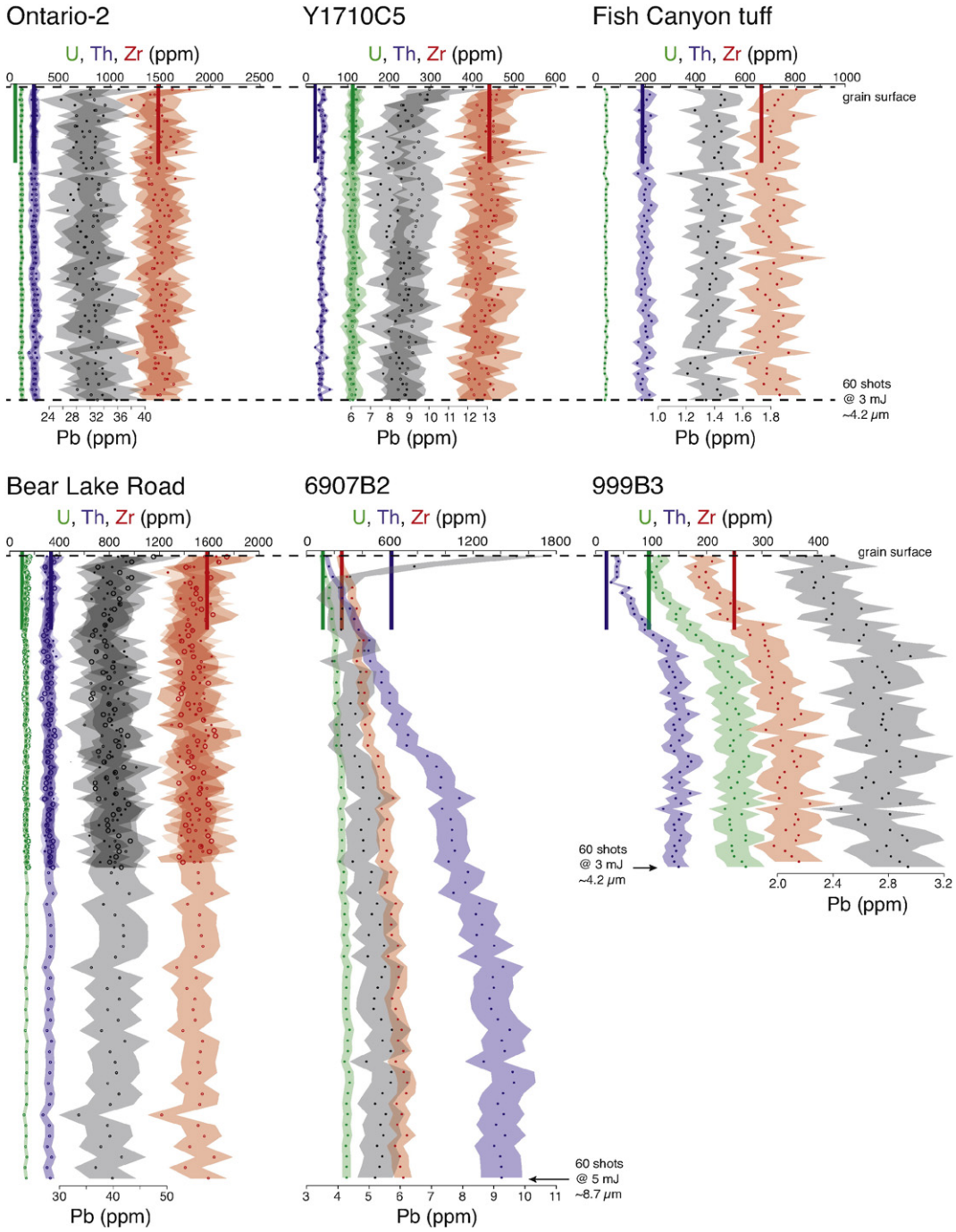

Fig. 6. Single-shot trace-element concentrations of the secondary reference titanites ONT-2, Y1710C5, Fish Canyon titanite, and Pamir Plateau samples 6907B2 and 999B3, plotted as a function of depth. The heavy solid green (U), purple (Th), red (Zr), and black (Pb) lines are the weighted mean EPMA analyses (this study). The lines extend to ~1 μm depth to indicate the likely interaction volume of the electron beam in the samples. The EPMA analyses uncertainty are less than the thickness of the lines.

instrument settings is in Table 1. The use of a static collector array, relative to using a single quadrupole or magnetic sector instrument, avoids lost counts due to long (>>200 ns) integration periods required of single collector instruments and settling time of quadrupole instruments while scanning between the seven masses used in this study.

Laser energy was stabilized prior to analysis by firing continuously for several minutes with a blocking shutter in place. Laser spots were placed on the flattest, inclusion-free portion of the grains (Fig. 3). Two cleaning shots were used to remove surface contamination (Fig. 3 inset); despite this, some samples show slightly elevated common Pb for the first few analyses. Each depth profile consists of 60 single laser-pulse analyses from a 54 μm diameter spot (Figs. 1 and 3). The amount of material ablated per laser pulse — the ablation efficiency — is expected to be constant under such conditions (van Soest et al., 2011) allowing the sampling depth of each laser pulse to be calculated from total pit depth. The final pit depths were measured using reflected-light microscopy and optical interferometry and found to be 4.2 ± 0.1 μm and 8.7 ± 0.1 μm for ~1.7 J/cm^2 and 2.8 J/cm^2, respectively. This is equivalent to ablation rates of ~67 and 145 nm/laser pulse or ~5,500 and ~11,800 ng of titanite per pulse; compare to ~240,000 ng of titanite in a traditional 80-shot laser ablation analysis at ~2 J/cm^2 using a 40 μm diameter spot. For titanite with 50 ppm Pb, a SS-LASS datum contains ~0.3–0.6 ng of total Pb compared to

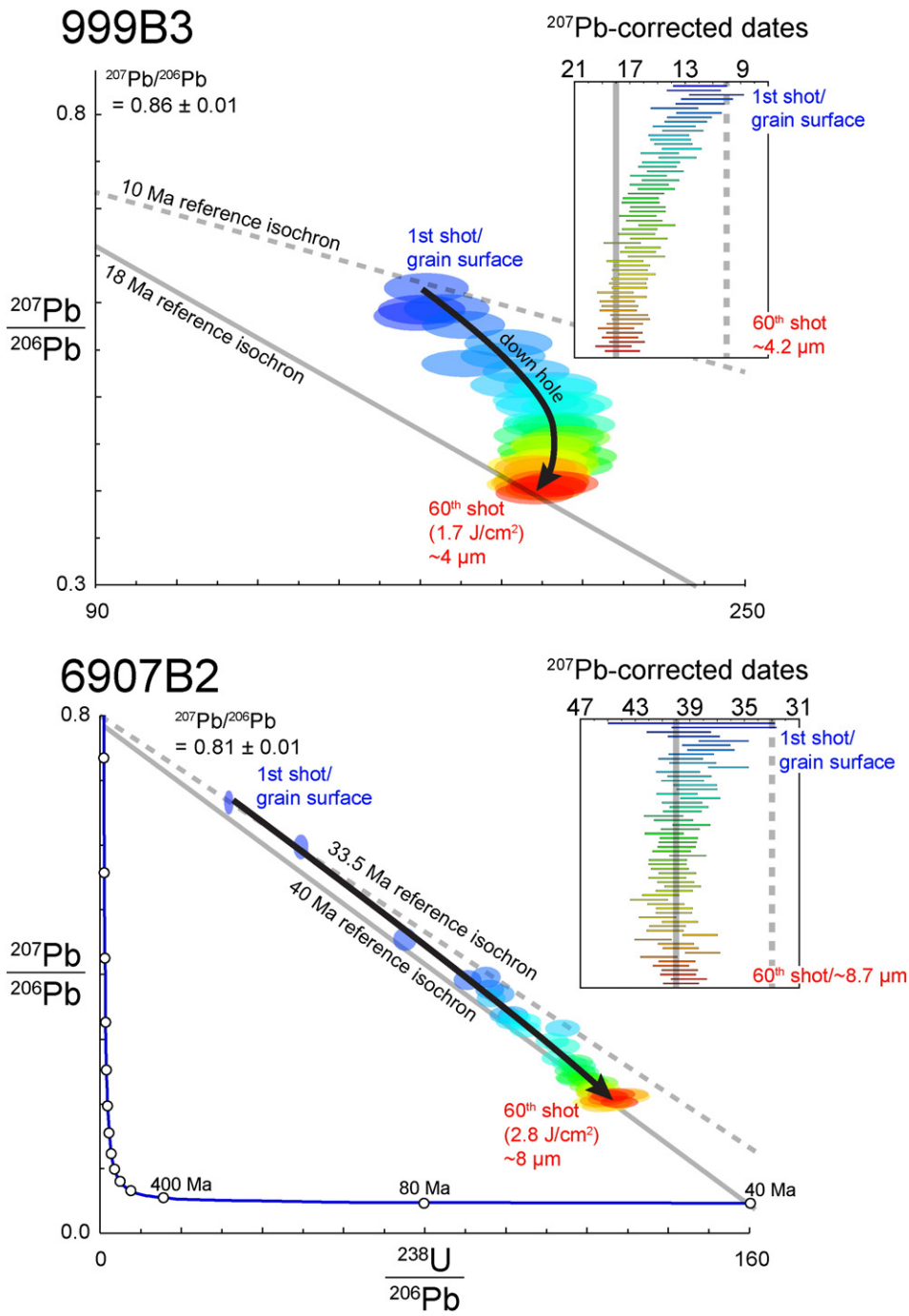

Fig. 7. Tera-Wasserburg concordia plots of Pamir titanites 999B3 and 6907B2 show the isotopic variation as a function of depth, each ellipse is a single laser shot. ^{207}Pb-corrected intercept dates (inset) are also plotted by depth from crystal surface. Purple indicates the 1st shot (near surface) and red the 60th laser shot. Grey lines are reference isochrons (Ludwig, 1998) to compare the trajectories of the data down the depth profile.

~12 ng Pb in a traditional analysis (~0.05–0.1 ng and ~2.4 ng Pb for 10 ppm Pb titanite, respectively).

Signal intensity in homogeneous reference materials typically decreases downhole by ~10–20%. Because of signal intensity decrease, use of either a larger spot, or polishing and further SS-LASS analysis would be necessary to obtain profiles deeper than ~10–15 μm. If the concentration or isotope ratio varies at a scale greater than ~30 μm, a line traverse of traditional laser spots across a medial section of a grain would better capture isotopic and chemical variation. Re-deposition of ablated material from early laser shots on the sample surface, pit sidewall, and pit bottom could potentially contaminate later shots. The amount of re-deposition has been shown to be a strong function of the number of laser pulses and the type of sample gas used during ablation (Eggins et al., 1998). Using fewer laser pulses and a helium atmosphere, rather than argon, significantly reduces re-deposition. It is also possible that laser pulses farther down the pit (shot 60 versus shot 5) experience a small amount of contamination from continued ablation of the sidewall material by subsequent laser pulses (Eggins et al., 1998). Both re-deposition on the surface and sidewall and contamination via continued sidewall ablation are minimized by the use of helium sample gas, the high aspect ratio of the analysis pit, and the >10 second waiting time between individual laser pulses.

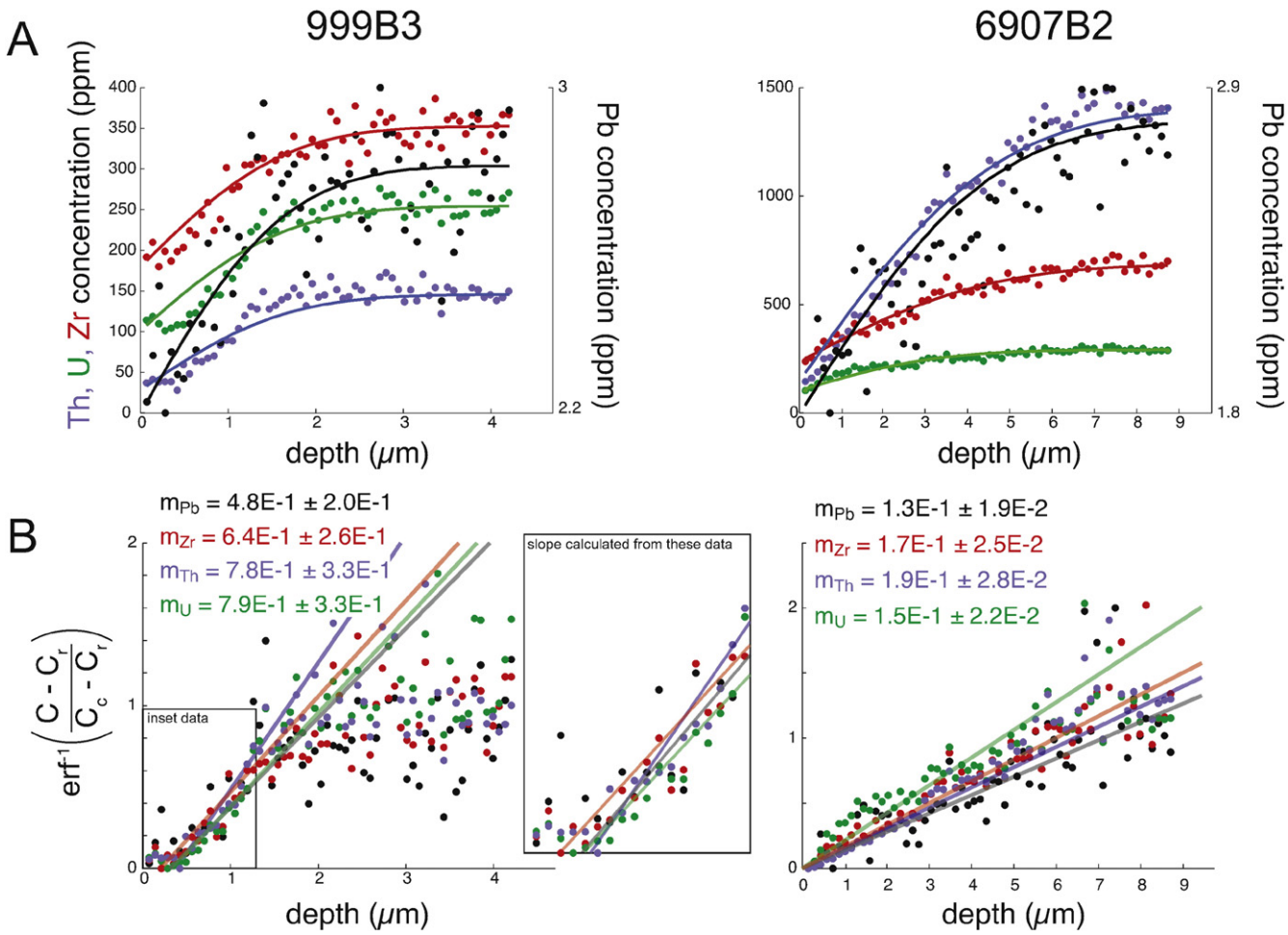

Fig. 8. The high spatial resolution of SS-LASS combined with semi-infinite source diffusion modeling gives insight into the process(es) controlling the near-surface trace element variation in titanite. A) The best-fit error function curves for experimentally determined diffusivities show reasonable fits when compared to the measured concentration profiles of Pb, Zr, Th, & U from the Pamir titanites, but require unreasonably short timescales (<300 kyr). B) Alternatively, the slopes of the inverted Pamir titanite data (Eq. (2)) and their best-fit linear regressions (proportional to D and t) are the same within error, eliminating lattice diffusion as the main process responsible for near-surface trace element variation of the Pamir titanites.

2.4. Data reduction

The raw data were reduced using a MATLAB® program, '*SLaPChron*' (Cottle et al., 2012), modified to process Zr, Pb, U, and Th concentrations in addition to the usual $^{207}Pb/^{206}Pb$, $^{238}U/^{206}Pb$, $^{235}U/^{207}Pb$ and $^{232}Th/^{208}Pb$ isotopic ratios. Corrections for down-hole elemental and inter-element fractionation, as well as a magnitude correction that adjusts the primary reference material to a known value, were completed in Microsoft Excel®. Time and depth-dependent elemental and inter-element fractionation were modeled via a linear regression of the primary reference material (BLR-1), which was then applied to all unknowns. Other regression types (grand mean, polynomial, and exponential) were investigated, but the linear regression routinely yields the best fit to the data with the lowest residuals. BLR-1 was used as the primary reference material because it provides a robust, matrix-matched down-hole correction and is isotopically homogeneous. Unfortunately a chemically homogeneous natural titanite reference material does not exist. BLR-1 is inhomogeneous at the grain scale with respect to U, Th, Pb, and Zr concentrations and requires characterization of each grain. The values of BLR-1 were thus measured by EPMA and further calibrated by comparing those measurements to BLR-1 values attained by normalizing to NIST-610 glass (Appendix 1). Due to the different down-hole fractionation behavior of glass and titanite, a surface intercept method was used when normalizing to NIST-610. This normalization assumes the least elemental fractionation occurs at the beginning of ablation. A standard-sample bracketing approach for each single laser shot of the primary and three secondary isotopic reference materials (BLR-1 & ONT-2, Y1710C5, FC-1 titanites), the primary and secondary trace element reference materials (NIST 610 glass and BLR-1 titanite), and unknown titanites (999B3 and 6907B2) during the analytical run provides several checks on the accuracy of the down hole elemental fractionation trends. The concentration values of Zr, Th, and U in BLR-1 obtained by normalizing to NIST-610 are within uncertainty of those measured by EPMA, confirming the robustness of this normalization scheme (Table 2). Throughout this study, the NIST-610 normalized and EPMA data for BLR-1 were utilized in preference to the published (Mazdab, 2009) trace element values for BLR-1.

Uncertainties in isotopic ratios and elemental concentrations were calculated using the population statistics of the primary reference titanite during each analytical run (one depth profile; see Cottle et al. (2012) for a description of error propagation). Each analysis consists of the summed total counts for a single laser pulse rather than repeat measurement of a homogeneous composition, and therefore – in contrast to traditional time-resolved data collection — gives a single datum with no associated external uncertainty. An external uncertainty for individual measurements (i.e. a single laser pulse) is computed as the quadratic sum of the counting statistics (internal uncertainty and usually the largest source of error) for the individual analysis plus two

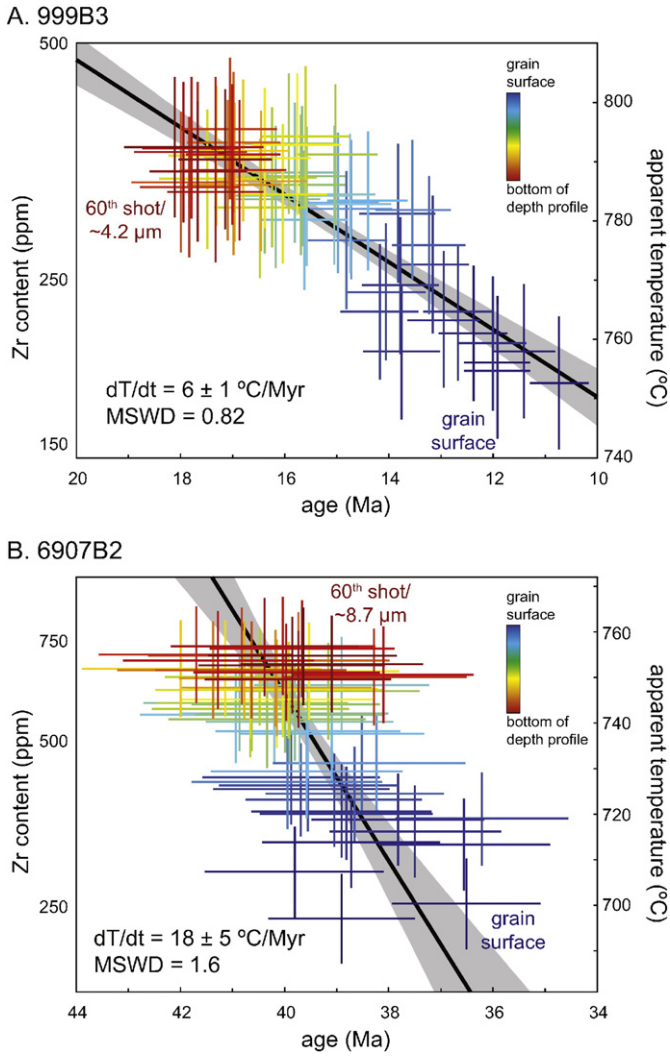

Fig. 9. If volume-diffusion loss can be eliminated, prolonged (re)crystallization-based cooling trajectories can be calculated from the U-Pb dates and apparent-Zr temperatures (Hayden et al., 2008). Linear regression of the data yields cooling rates of 6 ± 1 and 18 ± 5 °C/Myr for 999B3 and 6907B2, respectively. The cooling rate for 999B3 from ~19–11 Ma are slower than thermochronometrically determined rates of ~70 °C/Myr (for ~8–2 Ma; Stübner et al., 2013) for the same area, which may suggest an acceleration of tectonic unroofing of the Shakhdara dome between ~11–8 Ma.

standard deviations of the primary reference material mean value during a single analytical session (one depth profile). Additional uncertainty (typically ≤2%) is added in quadrature as required to make the secondary reference materials a single population (assuming a Gaussian distribution of uncertainties).

Isotopic ratios were plotted on Tera–Wasserburg concordia diagrams; in this space, the data typically form a linear array between initial or common Pb and radiogenic Pb that defines a SemiTotal-Pb/U isochron (Ludwig, 1998; Fig. 4). In Tera-Wasserburg space, titanites with intragrain age variation (i.e. young rim–old core) would likely manifest as curvilinear arrays with progressively lower $^{238}U/^{206}Pb$ ratios from rim to core. U-Pb ages were ^{207}Pb-corrected using the intercept method (York, 1966; Compston et al., 1992) and the initial or common-Pb composition defined by a group of co-genetic analyses, rather than ^{204}Pb, $^{208}Pb_{(no\ Th)}$ (Williams, 1998), or ^{202}Hg (Storey et al., 2006) based corrections. For data that do not define an isochron, such as the Pamir samples 999B3 and 6907B2, a common-Pb composition based on the Stacey and Kramers (1975) model for the approximate age of the sample was used. For reference, the upper-intercept values are reported in the upper left of the concordia diagrams.

Table 1
Instrument parameters.

Photon Machines 193nm ArF excimer laser	
Cell	Two volume Helex cell (Eggins et al., 1998, 2005)
Sample transport tubing	0.5–2 m length, Teflon
Washout time	<1 s
Wavelength	193 nm ArF
Energy (in software)	3 & 5 mJ
Fluence	~1.7 & 2.8 J cm^{-2}
Pulse width	<3 ns
Cell volume	3 cm^3
Drill depth/pulse	0.067 & 0.145 μm @ 54 μm diameter spot

	Nu Instruments 'HR Nu Plasma' MC-ICPMS	*Agilent 7700X Quadrupole-ICPMS*
Carrier gas flow rate	0.25 l min^{-1} (He) + 1.15 l min^{-1} Ar	1.15 l min^{-1} Ar
Auxiliary gas flow rate	0.8 l min^{-1} Ar	0.9 l min^{-1} Ar
Cool gas flow rate	13 l min^{-1} Ar	15 l min^{-1} Ar
RF power	1300 W	1350 W
Reflected power	<1 W	<1 W
Sample cone	Ni (1 mm orifice)	Ni (1 mm orifice)
Skimmer cone	Ni (0.7 mm orifice)	Ni (0.7 mm orifice)
Collectors	2 Faraday and 4 electron multipliers	dual-mode electron multiplier
Integration times	200 ms	100 ms
Isotopes measured	204Hg + Pb, 206, 207, 208Pb, 232Th, 238U	90Zr
Reference Materials	Bear Lake titanite (1047.4 ± 1.4 Ma; Aleinikoff et al., 2007), Y1710c5 titanite (385.8 ± 3.3 Ma; Spencer et al., 2013)	Bear Lake titanite (1300 ± 100 ppm Zr), NIST 610 glass (440 ± 16 ppm Zr)

2.5. Diffusion modeling

In general, the aim of diffusion modeling is to quantify rates of geologic processes using the movement of elements in response to chemical-potential gradients. In this study, the aim of diffusion modeling is to understand the first-order chemical and isotopic variation in the context of known diffusion parameters for titanite. We therefore adopt several simplifying assumptions: 1) Diffusion of the elements of interest is assessed by measuring and interpreting the concentration gradient of the elements; 2) Diffusion was isotropic; 3) Diffusivity was constant at a given pressure and temperature; 4) Diffusion can be modeled in a semi-infinite medium with a boundary condition of constant concentration at the grain surface because the titanite grain sizes in this study are ~100 times larger than the depth profile and; 5) The initial concentration of the diffusant was uniform in a semi-infinite medium and entirely captured within the depth profile (i.e. steady-state values are measured by the end of the depth profile).

For a semi-infinite source and constant diffusivity D, the normalized concentration profile at time t is given by Crank (1975):

$$\left(\frac{C-C_r}{C_c-C_r}\right) = erf\left(\frac{x}{\sqrt{4Dt}}\right) \tag{1}$$

where C is concentration, C_r rim concentration, C_c core concentration, x position, and D diffusivity. The normalized concentration data can be linearized with an inverse error function; the slope m of the inverted data is:

$$m = \frac{1}{\sqrt{4Dt}} \tag{2}$$

This relationship indicates that for a given time, temperature, and activation energy (E_a), the slopes of the inverted concentration profiles for different elements differ by $\sqrt{D}$. For titanite, at temperatures of

Table 2
Age and concentration data of reference materials and unknowns.

Sample	Author(s)	Method	Age (Ma)	±2σ (Ma)	Concentration (ppm)							
					Zr	±2σ	Pb	±2σ	U	±2σ	Th	±2σ
Bear Lake Road diggings	Spencer et al. (2013); Mazdab (2009); Aleinikoff et al. (2007)	ICP/EPMA	1047.4	1.4	1470/1300	-	19.7	-	300	-	186	-
	This study	EPMA	-	-	1485	25	-	-	75–99	20	319–355	13
		SS-ICP	I°	-	1491	157	40	4	134	14	319	34
Ontario-2	Spencer et al. (2013)	TIMS	1053.3	3.1	-	-	19–27	-	77–90		136–198	-
	this study	EPMA			1489	25	-	-	48	20	244	13
		SS-ICP	1065	37	1483	148	32	3	106	11	235	24
Y1710C5	Spencer et al. (2013)	TIMS/EPMA	385.8	3.3	128–229	-	-	-	-	-	-	-
	this study	EPMA			443	21	-	-	56	20	22	13
		SS-ICP	392	12	426	42	8.7	0.9	111	11	35	4
Fish Canyon titainte (FC-1)	Hayden et al. (2008); Bachmann et al. (2005); Schmitz and Bowring (2001)	TIMS/EPMA	28.53	0.05	576 & 596; 767	40	1.08–2.22	-	44–69	-	225–344; 400	-
	This study	EPMA			664	23	-	-	-	-	195	13
		SS-ICP	25.8	0.9	699	69	1.4	0.1	41	4	195	19
"Yates Mine" titanite	This study	EPMA	-	-	184	19	-	-	258	20	201	13
		SS-ICP	953	35	197	23	55	4.9	266	34	194	24
6907B2	Stearns et al. (2015)	ICP/EPMA	40.1	0.8	220–675	-	-	-	-	-	-	-
	This study	EPMA			275–366	20	-	-	71–283	21	608–735	14
		SS-ICP	42–36	-	128–553	13–56	3.7–5.7	0.4–0.6	104–310	12–33	145–1495	15–180
999B3	This study	EPMA	-	-	238–262	14	-	-	76–100	20	19, 415–459	14
		SS	18–10.7	-	180–387	20–40	2.2–3.0	0.2	101–276	12–30	28–172	3–18

500–900 °C, $D_{Pb} \approx 130\ D_{Zr}$ yielding $m_{Pb} \approx 12\ m_{Zr}$ (Cherniak, 1993; Chakraborty, 2006).

It is important to compare diffusants with similar activation energies (Cherniak et al., 1997) due to the kinetic effects of thermally activated diffusion. In other words, elements with similar E_a show similar temperature dependence, but diffuse at different rates. In titanite, Pb and Zr have similar E_a for lattice diffusion of 328 ± 11 kJ mol^{-1} and 321 ± 34 kJ mol^{-1}, respectively (Cherniak, 1993, 2006). Though no such experiments exist for diffusion of U or Th in titanite, the E_a for U and Th diffusion and zircon may provide a first-order approximation of the relative kinetic differences between Pb, U and Th. Experimentally determined E_a for U and Th diffusion in zircon are 726 ± 83 and 792 ± 34 kJ mol^{-1} respectively, which are ~30% higher than that of the E_a of Pb diffusion in zircon (Cherniak et al., 1997; Cherniak and Watson, 2001). Similarly, Sr and Nd diffusion in titanite have similar E_a, which are 40% higher than the E_a for Pb diffusion in titanite (Cherniak, 1993, 1995) and should therefore present good targets for assessing diffusion in titanite.

3. Results

3.1. Ontario-2

Single-shot dates of Ontario-2, one of three in-run secondary reference titanites analyzed to monitor external reproducibility during two analytical sessions (Fig. 5; 1062 ± 30 and 1064 ± 30 Ma), are in agreement with the previously published TIMS age of 1053 ± 3.1 Ma and LA-ICP-MS age of 1048.7 ± 2.6 Ma (Spencer et al., 2013). Measurements of Zr, Th, and Pb from the same two sessions are within ~10% of the EPMA values (Fig. 6 & Table 2) and in agreement with estimates of the U, Pb, and Th content based on TIMS measurements (Spencer et al., 2013). The EPMA measurement of U (48 ± 20 ppm) does not agree with the SS-LASS but is within error of the TIMS measurement – the latter has large uncertainties (~100%) from estimation of the masses of the grains prior to dissolution.

3.2. Y1710C5

Single-shot dates of secondary reference titanite Y1710C5, also analyzed in run during two analytical sessions (Fig. 5; 392 ± 12 and 400 ± 12 Ma), are within uncertainty of the published TIMS ages (Kylander-Clark et al., 2008; Spencer et al., 2013). Repeat analyses of U, Th, Pb, and Zr in Y1710C5 titanite from the same sessions form a single population. The average Zr concentration of 426 ± 42 ppm is equivalent to the EPMA measurements of the same grain (this study; Fig. 6 & Table 2) though lower than Spencer et al.'s (2013) EPMA measurement of a different grain. The Th content measured by SS-LASS differs from the EPMA measurement by 24%. The U contents measured by the two techniques agree within uncertainty.

3.3. Fish Canyon titanite

Fish Canyon tuff titanite have the lowest Pb concentrations (~1 ppm). Additionally, SS-LASS U-Pb data from the Fish Canyon tuff titanite are discordant and do not define an isochron and are thus difficult to interpret accurately. The SS-LASS trace-element measurements are in accord with published Zr, U, Th and Pb concentrations (Schmitz and Bowring, 2001; Bachmann et al., 2005; Hayden et al., 2008) and EPMA measurements (Table 2; this study).

3.4. Pamir titanite

Both Pamir samples exhibit coherent grain mantle to rim trends of the U-Pb isotopic compositions that indicate variation in age along the depth profile (Fig. 7). These trends are interpreted as three-component mixing of common Pb ($^{207}Pb/^{206}Pb \approx 0.8$, $^{238}U/^{206}Pb < 10$) and at least two radiogenic-Pb compositions ($^{207}Pb/^{206}Pb < 0.1$, $^{238}U/^{206}Pb \approx 160$ and 240 for samples 6907B2 and 999B3, respectively) that do not fall along partial-Pb isochrons (Ludwig, 1998). The isotopic ratios become more radiogenic and older (lower $^{207}Pb/^{206}Pb$ and $^{238}U/^{206}Pb$ ratios) downhole toward the center of the grain (Fig. 7).

For sample 999B3, the ^{207}Pb-corrected ages are ~10 Ma near the surface and reach a consistent age of ~18 Ma (~shot 50) near the bottom of the pit (Fig. 7A). Analyses of sample 6907B2 are nearly co-linear in Tera–Wasserburg space (Fig. 7B), but do not form a single population (MSWD = 2.2). The ^{207}Pb-corrected dates also do not form a single population (MSWD = 1.9). Like sample 999B3, the array is curved toward lower $^{238}U/^{206}Pb$ ratios with depth. The upper intercept of the first five shots was used to determine the composition of common Pb; using Stacey–Kramers common Pb as the upper intercept increases the ^{207}Pb-corrected dates by ~1.5%. While not statistically robust, the downward trend of decreasing $^{238}U/^{206}Pb$ is consistent with increasing

age and the trace-element zoning measured in this sample (see next section).

The trace-element concentrations of all elements measured in sample 999B3 increase from rim to grain mantle (Fig. 6): Zr from ~200 to 325 ppm, Th from ~40 to 150 ppm, U from ~110 to 250 ppm, and total Pb from ~2.3 to 2.8 ppm. The concentration of Th measured by EPMA was lower than the SS-LASS measurements by ~67%. This difference likely results from grain-scale heterogeneity within the sample. Each elemental profile has a similar shape: a homogeneous low-concentration rim (first six analyses, or 0–420 nm depth), a transition zone or mantle of increasing concentration (420–700 nm), and a homogeneous inner zone of higher concentration (700–3080 nm). The Zr concentrations correspond to apparent temperatures of 750–800 °C for a pressure of 8 kbar, chosen based on the barometry of similar-age, structurally similar rocks, (Schmidt et al., 2011). When modeling the trace element distribution in sample 999B3, the homogenous low-concentration rim (i.e. analyses 1–5) was excluded from the inversion, thus the linear best-fit model has a negative y-intercept.

The trace-element concentrations of all elements measured in sample 6907B2 increase from rim to mantle (Fig. 6): Zr from ~125 to 550 ppm, Th from ~150 to 1500 ppm, U from ~105 to 310 ppm, and total Pb from ~3.7 to 5.7 ppm. Each elemental profile has a similar shape: low concentration rim that increases rapidly toward a homogeneous grain mantle. The Zr concentrations correspond to apparent temperatures of 700–770 °C for an assumed pressure of 3 kbar based on a reasonable estimate of the pre-thickening emplacement pressure for rocks now within the Yazgulem dome (Schmidt et al., 2011).

4. Discussion

4.1. Interpretation of the elemental gradients

If the measured concentration gradients are the result of volume diffusion, each element gradient that satisfies the simplifying assumptions should define a unique $\frac{1}{\sqrt{4Dt}}$ slope that scales with the element diffusivity. In particular, as noted above for titanite, $m_{Pb} \approx 12\ m_{Zr}$. Fig. 8 illustrates that when the concentration gradients are inverted through erf^{-1}, both of the element pairs – and, importantly Pb and Zr – define the same $\frac{1}{\sqrt{4Dt}}$ slope ($4.8 \pm 2.0 \times 10^{-1}$ and $6.4 \pm 2.6 \times 10^{-1}$ respectively). Additionally, one-dimensional diffusion distance calculations ($x = \sqrt{2Dt}$; using an appropriate D for the apparent Zr temperatures) predict that Pb should diffuse tens to hundreds of microns during cooling – 11x and 12x the expected diffusion distance of Zr for samples 6907B2 and 999B3, respectively. Additionally, Pb and Zr are unlikely to diffusively "uncouple" because of the similar activation energies.

The measured concentration gradients *within* the measured depth profile are not consistent with the predicted volume diffusion of Pb and Zr in titanite. Instead, process(es) other than volume diffusion, such as local chemical depletion during prolonged crystallization or modification via titanite recrystallization, are likely responsible for the observed near-rim zoning. Kohn and Corrie (2011) documented similar near-rim isotopic and chemical zoning in titanites from the Greater Himalayan Sequence in Nepal, which they interpreted as prolonged growth of titanite during prograde metamorphism.

In contrast to the continuous drilling methods of Kohn and Corrie (2011) and Smye and Stockli (2014), the SS-LASS method enables U-Pb isotopic and concentration data to be obtained from each single datum/laser shot. This eliminates the need to bin or average analyses for error propagation and affords finer scale depth resolution. The complete counting and return to background after a single laser shot also eliminates the effect of washout on the correlation between isotopic composition and concentration data. The use of BLR-1 as a single primary reference material (e.g., Kohn and Corrie, 2011) provides robust matrix matching behavior, but relies on a material that has been shown to have trace-element heterogeneity at the grain scale. External calibration via EPMA and the use of the secondary reference material during SS-LASS in this study provide a further means of assessing the accuracy of the trace-element concentrations.

These data demonstrate that modeling the concentration profile of a single element in order to quantify timescales of geologic processes can be perilous because of the non-unique nature of a model that depends on both time and diffusivity. Profiles of multiple elements with a range of diffusivities (and similar E_a) provide a more-robust approach for extracting thermal histories from diffusion profiles (Watson and Cherniak, 2015). One of the strengths of multi-element depth profiling lies in the ability to assess whether the concentration gradients of elements with different diffusivities lead to the same inferred thermal history. The data presented here show that the volume-diffusion cooling histories calculated from a single-element profiles are: 1) too short given range of U-Pb dates and Zr concentration captured within the profiles and; 2) inconsistent between elements pairs with similar E_a (i.e. kinetic behavior; Pb & Zr, U & Th) given the laboratory derived diffusivities and the non-uniqueness of the error function solution to the diffusion equation resulting from incomplete temperature time histories, initial and boundary conditions for these natural titanites. For example, calculating the temperature and time by fitting the concentration profiles in 6907B2 titanite leads to values of 750 °C for ~300 yr for Pb and ~30 kyr for Zr, which when compared to the ~15 Myr and ~27 Myr duration of titanite (re)crystallization in the Yazgulem and Shakhdara domes, respectively (Stearns et al., 2015; Stübner et al., 2013) are geological improbable. Rather, the U-Pb dates and Zr thermometry are consistent with other thermochronology data from similar rocks (Fig. 8A; Rutte et al., 2013; Stübner et al., 2013). It is possible that larger, grain-scale diffusion profiles are present that were not captured within the depth profiles presented here.

If the measured elemental concentration gradients are not the result of volume diffusion, they may instead be the result of growth zoning during protracted (re)crystallization and reflect time-dependent changes in partitioning of Th, U, Pb and Zr into titanite. All of the elements, despite the wide variety of predicted diffusive behavior, vary at the same length scale. This suggests that the variation of all of the measured elements in 999B3 and 6907B2 is sensitive to the same mechanism. Some possible mechanisms are changing equilibrium (Prowatke and Klemme, 2005) or disequilibrium partitioning (Paterson and Stephens, 1992) during prolonged crystallization, and/or changes in pressure or temperature during protracted (re)crystallization (Hayden et al., 2008). Distinguishing among these mechanisms is difficult, especially given that the context of the grain has been lost due to mineral separation. The truncated high-concentration mantle surrounded by a homogeneous low-concentration ~0.5 μm rim in sample 999B3 more closely resembles modification by recrystallization. This would be consistent with alteration during retrograde metamorphism documented in other samples from the southern Shakhdara dome (Stearns et al., 2015). Alternatively, the limited range of U-Pb dates and the more continuous variation in the zoning of sample 6907B2 titanite perhaps more likely represents time-dependent changes in partitioning during crystallization from a melt. These interpretations are speculative in nature and more detailed petrology in the context of surrounding phases and textures of both samples would be needed to make more robust interpretations.

If the zoning in both 999B3 and 6907B2 represents protracted (re)-crystallization – and if not modified by diffusion or another process – reliable cooling rates based on protracted (re)crystallization and equilibration can be extracted from the zoning by combining U-Pb ages and Zr apparent temperatures from each datum of the depth profile (Fig. 9). Cooling rates calculated from linear regression of the data are ~6 ± 1 °C/Myr from ~18–11 Ma for 999B3 and ~18 ± 5 °C/Myr from ~41–37 Ma for 6907B2. These cooling rates are geologically reasonable and consistent with existing $^{40}Ar/^{39}Ar$, fission track, and U-Th/He thermochronology studies that show much faster cooling rates in both the southern Shakhdara dome (Stübner et al., 2013) and Central

Pamir domes (Rutte et al., 2013, 2014) following ~11 and ~20 Ma, respectively. Multi-phase cooling ages (Ar-Ar mica, zircon and apatite fission track, and U/Th-He zircon and apatite) from near sample 999B3 indicate a faster post-11 Ma cooling rate of ~70 ± 16 °C/Myr from ~8 to ~2 Ma of Stübner et al. (2013). These two independent cooling rates indicate a transition to more rapid cooling between ~11 and 8 Ma, and provide tighter limits on the timing of tectonic events than either thermochronometer alone.

5. Conclusions

Single shot-LASS depth profiling is capable of accurately and precisely (~5–10%) determining the U-Pb age and trace element concentrations in titanite with ~100 nm spatial resolution. Furthermore, the role of lattice diffusion in titanite can be evaluated by modeling the near-rim trace-element zoning using a simple semi-infinite, half-space diffusion model. For internal consistency, it is necessary to measure multiple trace elements with different diffusivities to interpret a mineral's thermal history. Pamir titanite that experienced prolonged amphibolite to lower-granulite facies metamorphism apparently did not experience significant lattice diffusion modification, but rather retained their U-Pb ages and trace element distribution related to (re)crystallization. Additionally, if lattice-diffusion processes can be ruled out and instead the titanites record protracted (re)crystallization, detailed temperature-time histories can be extracted from the concurrently measured U-Pb dates and Zr^{4+} apparent temperatures.

Acknowledgements

NSF grants EAR-0838269, EAR-1050043, and EAR-1119380 funded this research. We would like to acknowledge and thank Hans Vrijmoed for help with the programming of '*SLaPChron*'.

Appendix A. Supplementary data

Supplementary data to this article can be found online at http://dx.doi.org/10.1016/j.chemgeo.2015.12.011.

References

Abbott, S.S., Harrison, T.M., Schmitt, A.K., Mojzsis, S.J., 2012. A search for thermal excursions from ancient extraterrestrial impacts using Hadean zircon Ti-U-Th-Pb depth profiles. PNAS 109, 13486–13492. http://dx.doi.org/10.1073/pnas.1208006109.

Aleinikoff, J.N., Wintsch, R.P., Tollo, R.P., Unruh, D.M., Fanning, C.M., Schmitz, M.D., 2007. Ages and origins of rocks of the Killington dome, south-central Connecticut: Implications for the tectonic evolution of southern New England. Am. J. Sci. 307, 63–118. http://dx.doi.org/10.2475/01.2007.04.

Bachmann, O., Dungan, M.A., Bussy, F., 2005. Insights into shallow magmatic processes in large silicic magma bodies: the trace element record in the Fish Canyon magma body, Colorado. Contrib. Mineral. Petrol. 149, 338–349.

Bonamici, C.E., Fanning, C.M., Kozdon, R., Fournelle, J.H., Valley, J.W., 2015. Combined oxygen-isotope and U-Pb zoning studies of titanite: New criteria for age preservation. Chem. Geol. 398, 70–84. http://dx.doi.org/10.1016/j.chemgeo.2015.02.002.

Chakraborty, S., 2006. Diffusion modeling as a tool for constraining timescales of evolution of metamorphic rocks. Mineral. Petrol. 88, 7–27. http://dx.doi.org/10.1007/s00710-006-0152-6.

Cherniak, D.J., 1993. Lead diffusion in titanite and preliminary results on the effects of radiation damage on Pb transport. Chem. Geol. 110 (1), 177–194.

Cherniak, D.J., 1995. Sr and Nd diffusion in titanite. Chem. Geol. 125 (3–4), 219–232. http://dx.doi.org/10.1016/0009-2541(95)00074-V.

Cherniak, D.J., 2006. Zr diffusion in titanite. Contrib. Mineral. Petrol. 152 (5), 639–647.

Cherniak, D.J., Watson, E.B., 2001. Pb diffusion in zircon. Chem. Geol. 172, 5–24. http://dx.doi.org/10.1016/S0009-2541(00)00233-3.

Cherniak, D.J., Hanchar, J.M., Watson, E.B., 1997. Diffusion of tetravalent cations in zircon. Contrib. Mineral. Petrol. 127, 383–390. http://dx.doi.org/10.1007/s004100050287.

Compston, W., Williams, I.S., Kirschvink, J.L., Zichao, Z., Guogen, M.A., 1992. Zircon U-Pb ages for the Early Cambrian time-scale: Journal of the Geological Society. vol. 149 pp. 171–184. http://dx.doi.org/10.1144/gsjgs.149.2.0171.

Cottle, J.M., Searle, M.P., Horstwood, M.S.A., and Waters, D.J., 2009, Timing of midcrustal metamorphism, melting, and deformation in the Mount Everest region of southern Tibet revealed by U(-Th)-Pb geochronology: J. Geol., v. 117, p. 643–664, http://dx.doi.org/10.1086/605994.

Cottle, J.M., Kylander-Clark, A.R., Vrijmoed, J.C., 2012. U-Th/Pb geochronology of detrital zircon and monazite by single shot laser ablation inductively coupled plasma mass spectrometry (SS-LA-ICPMS). Chem. Geol. 332–333, 136–147. http://dx.doi.org/10.016/j.chemgeo.2012.09.035.

Crank, J., 1975. The mathematics of diffusion: Uxbridge. Brunel University Press, p. 414.

Dodson, M.H., 1973. Closure temperature in cooling geochronological and petrological systems. Contrib. Mineral. Petrol. 40, 259–274.

Eggins, S.M., Kinsley, L.P.J., Shelley, J.M.G., 1998. Deposition and element fractionation processes during atmospheric pressure laser sampling for analysis by ICP-MS. Appl. Surf. Sci. 127–129, 278–286. http://dx.doi.org/10.1016/S0169-4332(97)00643-0.

Eggins, S.M., Grün, R., McCulloch, M.T., Pike, A.W.G., Chappell, J., Kinsley, L., Mortimer, G., Shelley, M., Murray-Wallace, C.V., Spötl, C., Taylor, L., 2005. In situ U-series dating by laser-ablation multi-collector ICPMS: new prospects for Quaternary geochronology: Quaternary Science Reviews. vol. 24 pp. 2523–2538. http://dx.doi.org/10.1016/j.quascirev.2005.07.006.

Frost, B.R., Chamberlain, K.R., Schumacher, J.C., 2001. Sphene (titanite): phase relations and role as a geochronometer. Chem. Geol. 172 (1), 131–148.

Gao, S., Liu, X., Yuan, H., Hattendorf, B., Günther, D., Chen, L., Hu, S., 2002. Determination of Forty Two Major and Trace Elements in USGS and NIST SRM Glasses by Laser Ablation-Inductively Coupled Plasma-Mass Spectrometry. J. Geostandard. Geoanal. 26, 181–196.

Grove, M., Harrison, T.M., 1999. Monazite Th-Pb age depth profiling. Geology 27, 487–490. http://dx.doi.org/10.1130/0091-7613(1999)027<0487:MTPADP>2.2.CO.2.

Harlov, D., Tropper, P., Seifert, W., Nijland, T., Förster, H.J., 2006. Formation of Al-rich titanite ($CaTiSiO_4O$–$CaAlSiO_4OH$) reaction rims on ilmenite in metamoprhic rocks as a function of fH_20 and fO_2. Lithos 88, 72–84. http://dx.doi.org/10.1016/j.lithos.2005.08.005.

Hayden, L.A., Watson, E.B., Wark, D.A., 2008. A thermobarometer for sphene (titanite). Contrib. Mineral. Petrol. 155 (4), 529–540.

Kelley, C.J., McFarlane, C.R.M., Schneider, D.A., Jackson, S.E., 2014. Dating micrometre-thin rims using a LA-ICP-MS depth profiling technique on zircon from an Archaean metasediment: Comparison with the SIMS depth profiling method. Geostandard. Anal. Res. 38, 389–407. http://dx.doi.org/10.1111/j.1751-908X.2014.00314.x.

Kohn, S.L., Corrie, M.J., 2011. Preserved Zr-temperatures and U-Pb ages in high-grade metamorphic titanite: Evidence for a static hot channel in the Himalayan orogen. Earth Planet. Sci. Lett. 311, 136–143. http://dx.doi.org/10.1016/j.epsl.2011.09.008.

Kylander-Clark, A.R.C., Hacker, B.R., Mattinson, J.M., 2008. Slow exhumation of UHP terranes: Titanite and rutile ages of the Western Gneiss Region, Norway. Earth Planet. Sci. Lett. 272, 531–540. http://dx.doi.org/10.1016/j.epsl.2008.05.019.

Kylander-Clark, A.R.C., Hacker, B.R., Cottle, J.M., 2013. Laser-ablation split-stream ICP petrochronology. Chem. Geol. 345, 99–112. http://dx.doi.org/10.1016/j.chemgeo.2013.02.019.

Lee, J.K.W., Williams, I.S., Ellis, D.J., 1997. Pb, U and Th diffusion in natural zircon. Nature 390, 159–162. http://dx.doi.org/10.1038/36554.

Ludwig, K.R., 1998. On the treatment of concordant Uranium–Lead ages: Geochimica et Cosmochimica Acta. vol. 62 pp. 665–676. http://dx.doi.org/10.1016/S0016-7037(98)00059-3.

Mazdab, F.K., 2009. Characterization of flux-grown trace-element-doped titanite using the high-mass-resolution ion microprobe (SHRIMP–RG). Can. Mineral. 47 (4), 813–831.

Parrish, R.R., Gough, S.J., Searle, M.P., Waters, D.J., 2006. Plate velocity exhumation of ultrahigh-pressure eclogites in the Pakistan Himalaya. Geology 34, 989–992. http://dx.doi.org/10.1130/G22796A.1.

Paterson, B.A., Stephens, W.E., 1992. Kinetically induced compositional zoning in titanite: implications for accessory-phase/melt partitioning of trace elements. Contrib. Mineral. Petrol. 109, 373–385. http://dx.doi.org/10.1007/BF00283325.

Prowatke, S., Klemme, S., 2005. Effect of melt composition on the partitioning of trace elements between titanite and silicate melt. Geochim. Cosmochim. Acta 69, 695–709. http://dx.doi.org/10.1016/j.gca.2004.06.037.

Rubatto, D., Hermann, J., 2001. Exhumation as fast as subduction? Geology 29, 3–6. http://dx.doi.org/10.1130/0091-7613(2001)029<0003:EAFAS>2.0.CO;2.

Rutte, D., Stearns, M., Ratschbacher, L., 2013. The eastern Central Pamir Gneiss Domes: temporal and spatial geometry of burial and exhumation. EGU General Assembly Conference Abstracts vol. 15, p. 6090.

Rutte, D., Ratschbacher, L., Schneider, S., Stearns, M., 2014. Shortening and syn-contractional extension: the burial and exhumation history of the Cenozoic Central Pamir Gneiss domes, Tajikistan. EGU General Assembly Conference Abstracts vol. 16, p. 11562.

Schmitz, M.D., Bowring, S.A., 2001. U-Pb zircon and titanite systematics of the Fish Canyon Tuff: an assessment of high-precision U-Pb geochronology and its application to young volcanic rocks. Geochim. Cosmochim. Acta 65, 2571–2587. http://dx.doi.org/10.1016/S0016-7037(01)00616-0.

Schmidt, J., Hacker, B.R., Ratschbacher, L., Stübner, K., Stearns, M.A., Kylander-Clark, A.R.C., Cottle, J.M., Alexander, A., Webb, G., Gehrels, G., Minaev, V., 2011. Cenozoic deep crust in the Pamir: Earth and Planetary Science Letters. vol. 312 pp. 411–421. http://dx.doi.org/10.1016/j.epsl.2011.10.034.

Schwab, M., Ratschbacher, L., Siebel, W., McWilliams, M., Minaev, V., Lutkov, V., Chen, F., Stanek, K., Nelson, B., Frisch, W., Wooden, J.L., 2004. Assembly of the Pamirs: Age and origin of magmatic belts from the southern Tien Shan to the southern Pamirs and their relation to Tibet. Tectonics 23, TC4002. http://dx.doi.org/10.1029/2003TC001583.

Scott, D.J., St-Onge, M.R., 1995. Constraints on Pb closure temperature in titanite based on rocks from the Ungava orogen, Canada: Implications for U-Pb geochronology and PTt path determinations. Geology 23 (12), 1123–1126.

Smit, M.A., Ratschbacher, L., Kooijman, E., Stearns, M.A., 2014. Early evolution of the Pamir deep crust from Lu-Hf and U-Pb geochronology and garnet thermometry. Geology 42, 1047–1050. http://dx.doi.org/10.1130/G35878.1.

Smye, A.J., Stockli, D.F., 2014. Rutile U-Pb age depth profiling: A continuous record of lithospheric thermal evolution. Earth Planet. Sci. Lett. 408, 171–182. http://dx.doi.org/10.1016/j.epsl.2014.10.013.

Spear, F.S., 1981. Amphibole-plagioclase equiibria: An empirical model for the relation albite + tremolite = edenite + 4 quartz. Contrib. Mineral. Petrol. 77, 355–364.

Spencer, K.J., Hacker, B.R., Kylander-Clark, A.R.C., Andersen, T.B., Cottle, J.M., Stearns, M.A., Poletti, J.E., Seward, G.G.E., 2013. Campaign-style titanite U-Pb dating by laser-ablation ICP: Implications for crustal flow, phase transformations and titanite closure. Chem. Geol. 341, 84–101. http://dx.doi.org/10.1016/j.chemgeo.2012.11.012.

Stacey, J.S., Kramers, J.D., 1975. Approximation of terrestrial lead isotope evolution by a two-stage model. Earth Planet. Sci. Lett. 26, 207–221. http://dx.doi.org/10.1016/0012-0821X(75)90088-6.

Stearns, M.A., Hacker, B.R., Ratschbacher, L., Lee, J., Cottle, J.M., Kylander-Clark, A.R.C., 2013. Synchronous Oligocene–Miocene metamorphism of the Pamir and the north Himalaya driven by plate-scale dynamics: Geology. vol. 41 pp. 1071–1074. http://dx.doi.org/10.1130/G34451.1.

Stearns, M.A., Hacker, B.R., Ratschbacher, L., Rutte, D., Kylander-Clark, A.R.C., 2015. Titanite petrochronology of the Pamir gneiss domes: Implications for mid–deep crust exhumation and titanite closure to Pb and Zr diffusion. Tectonics 34, 1–19. http://dx.doi.org/10.1002/2014TC003774.

Storey, C.D., Jeffries, T.E., Smith, M.P., 2006. Common lead-corrected laser ablation ICP–MS U–Pb systematics and geochronology of titanite. Chem. Geol. 227, 37–52. http://dx.doi.org/10.1016/j.chemgeo.2005.09.003.

Stübner, K., Ratschbacher, L., Weise, C., Chow, J., Hofmann, J., Khan, J., Rutte, D., Sperner, B., Pfänder, J.A., Hacker, B.R., Dunkl, I., Tichomirowa, M., Stearns, M.A., Project TIPAGE members, 2013. The giant Shakhdara migmatitic gneiss dome, Pamir, India-Asia collision zone: 2. Timing of dome formation. Tectonics 32 (5), 1404–1431. http://dx.doi.org/10.1002/tect.20059.

van Soest, M.C., Monteleone, B.D., Hodges, K.V., Boyce, J.W., 2011. Laser depth profiling studies of helium diffusion in Durango fluorapatite: Geochimica et Cosmochimica Acta. vol. 75 pp. 2409–2419. http://dx.doi.org/10.1016/j.gca.2011.02.008.

Viete, D.R., Kylander-Clark, A.R.C., Hacker, B.R., 2015. Single-shot laser ablation split stream (SS-LASS) petrochonology deciphers multiple, short-duration metamorphic events. Chem. Geol. 415, 70–86. http://dx.doi.org/10.1016/j.chemgeo.2015.09.013.

Watson, E.B., Cherniak, D.J., 2015. Quantitative cooling histories form stranded diffusion profiles. Contrib. Mineral. Petrol. 169 (57). http://dx.doi.org/10.1007/s00410-015-1153-4.3 (14 pp.).

Williams, I.S., 1998. Chapter 1. U–Th–Pb geochronology by ion microprobe. In: Mckibben, M.A., Shanks III, W.C., Ridley, W.I. (Eds.), Applications of Microanalytical Techniques to Understanding Mineralizing processes, Reviews in Economic Geology. Soc. Econom. Geol. Inc., Littleton, CO.

York, D., 1966. Least-squares fitting of a straight line. Can. J. Phys. 44, 1079–1086. http://dx.doi.org/10.1139/p66-090.

Zhang, L.S., Schärer, U., 1996. Inherited Pb components in magmatic titanite and their consequence for the interpretation of U-Pb ages. Earth Planet. Sci. Lett. 138, 57–65. http://dx.doi.org/10.1016/0012-821X(95)00237-7.